



SCIREA Journal of Energy

ISSN: 2995-7737

<http://www.scirea.org/journal/Energy>

June 1, 2025

Volume 10, Issue 1, February 2025

<https://doi.org/10.54647/energy480253>

Performance Testing of a Modified Double Slope Solar Still with PCM Filled Hollow Coil Fins: Assessing Energy, Exergy, Exergo-Economic, Environmental Analysis

Lailatul Nehar^{a b}, Tanvir Rahman^{a*}, Md Shahiduzzaman Shahed^a, Md Yeamin Prodhan^a, Md Sazan Rahman^{a c}, S. S. Tuly^a

^a Department of Mechanical Engineering, Rajshahi University of Engineering & Technology, Rajshahi, 6204, Bangladesh

^b Department of Industrial & Production Engineering, National Institute of Textile Engineering & Technology, Savar, Bangladesh

^c Department of Agriculture, Nutrition, and Food Systems, University of New Hampshire, Durham 03824, NH, USA

**Corresponding author contact details: email: tttanvirrrr@gmail.com, telephone: +8801754064645.*

Abstract

Solar still, while cost-effective and energy-efficient, often face limitations in productivity that hinder its usability in fresh water supply. Several performance enhancement methods for solar stills are explored in this study through different modifications. Three configurations were examined: a conventional double slope solar still (Case I), a solar still with hollow copper coil-

shaped fins (Case II), and a solar still with PCM filled hollow copper coil-shaped fins (Case III). Experimental investigations were conducted to assess the energy, exergy, economic, and environmental performance of these systems. The results indicate that integrating hollow copper coil-shaped fins significantly improved productivity, with Case II achieving a notable increase compared to the conventional one. However, the most substantial enhancement was observed in Case III, where the combination of hollow copper coil-shaped fins and PCM led to the highest productivity boost. Case III also demonstrated the most significant improvements in energy and exergy efficiencies, surpassing both the conventional and the fin-only configuration. Specifically, the use of PCM filled copper coil-shaped fins resulted in the highest yield of 1790 ml/day, where the conventional solar still produced 590 ml/day of fresh water. Further analysis revealed that the PCM-filled coil-shaped fins also contributed to cost savings and reduced environmental impact, including a reduction in CO₂ emissions. The exergy sustainability indicators for the three cases showed that Case III provided the highest values in terms of improvement potential and sustainability index. In summary, the integration of PCM filled hollow coil-shaped fins with the double slope solar stills results in superior performance, demonstrating the highest efficiency and productivity improvements among the configurations tested.

Keywords: CO₂ mitigation; copper coil fin; energy analysis; exergy analysis; PCM; Solar still.

1. Introduction

Freshwater scarcity is one of the most critical global issues where the demand for clean and accessible water surpasses the available supply. Numerous regions are grappling with severe water shortages due to rapid population growth, climate change, and pollution. As freshwater resources like rivers, lakes, and aquifers become depleted or contaminated, billions of people struggle to meet their daily water needs [1]. This scarcity not only limits the availability of drinking water but also impacts agriculture, industry, and overall economic development, leading to significant social and environmental repercussions. Approximately 2.2 billion people worldwide lack access to safely managed drinking water, 4.2 billion people do not have access to safely managed sanitation services, and 3 billion people lack basic handwashing facilities.

Furthermore, 22% of healthcare facilities in developing nations have no water services, 21% lack sanitation services, and 22% have no waste treatment services [2].

Desalination is one of the most effective methods to produce potable water from brackish or seawater [3]. Various techniques for water purification exist, often relying on chemical or electrical energy for desalination. However, solar distillation technology offers a cost-effective and environmentally friendly alternative [4]. The solar still offers fresh water consistently from saline water through its evaporation–condensation process, after effectively removing dissolved salts, impurities, and suspended solids [5]. Solar stills are generally categorized into passive and active types [6]. Due to the low productivity of conventional solar stills, extensive research has been conducted globally to enhance their efficiency by assessing the influence of critical factors such as climate, operational conditions, structural parameters, and geographical location [7]. The efficiency of solar stills depends on various operational parameters (such as basin content, exposure area, water and glass temperatures, water inlet temperature, water depth, and cover inclination) and meteorological parameters (wind speed, ambient temperature, and solar intensity) [8]. Therefore, the thermal performance and effectiveness of solar stills can be improved by modifying the structural parameters and/or adjusting operational conditions. Numerous design modifications have been proposed to enhance solar still productivity, including double slope receivers [9], pyramid solar stills [10], stepped solar stills [11], spherical [12], and hemispherical solar stills [13]. Further performance enhancements have been suggested through the addition of fins [14], internal and external reflectors [15], and cover cooling techniques [16].

Recent research advancements in solar distillation have focused on integrating thermal energy storage materials other than water to boost the efficiency of distillation units. Thermal energy storage media capture and store solar thermal energy in the form of sensible heat, latent heat, or both, which can be utilized to produce fresh water for industrial, building, and solar distillation applications [17]. The main advantages of using thermal energy storage include increase overall efficiency, improve economic viability, reduce operational costs, and enhance reliability. Consequently, the potential use of phase change materials (PCMs) as thermal energy storage media in solar system applications has been justified through several investigations [18]. Researchers have increasingly explored the use of PCMs to improve solar still output. Nano-enhanced phase change materials have been tested to test their thermophysical properties and applications on solar distillation use and notable increase in productivity had been observed [20].

Experiments were conducted to use PCM as thermal energy storage to increase productivity during dark hours [21]. A hybrid mechanism (magnetic and solar-driven energy conversion) utilizing PCM demonstrated excellent thermal stability, high melting-freezing enthalpy, and superior reversibility [22]. A sunlight-driven thermoelectric system with temperature difference control exhibited ultrafast photothermal conversion of the PCM through nonradiative decay of the excited state, effectively harnessing solar radiation [23]. Usage of PCM in solar still also introduced various challenges such as high cost, storage and leakage problem and longtime stability [24,25]. Although PCMs significantly enhance solar still yield, they often suffer from high volumetric expansion ratios and low thermal conductivity [26]. Heat conductivity of PCMs can be further increased by incorporating fins with absorber plate and mixing nanoparticles such as Al₂O₃ with conventional PCM like wax [27]. The addition of nano-PCMs and PCMs enhanced freshwater productivity by 67.07% and 51.22%, respectively, compared to conventional solar stills [28]. Safaei et al. [29] utilized graphene oxide/paraffin nano-PCMs to improve the productivity of solar still desalination processes.

Research has been conducted to test various fin configurations in solar stills (SS) to enhance productivity. For any single basin solar still (SBSS), the output of finned SS improves with increased fin height but decreases with a higher number of fins and fin thickness [30]. The productivity was enhanced by 75% when a SBSS was integrated with five solid rectangular fins, pebbles, sand, black rubber, and sponges for purifying industrial wastewater [31]. The use of square and circular fins in SBSS yielded 26.3% and 36.7% higher pure water than conventional solar stills [32]. Various fin materials (aluminum, glass, copper, mica, stainless steel, brass, and iron) have been used to test the performance of solar stills [33]. Omara et al. [34] compared the effects of corrugated and vertical fins on solar stills and found 21% and 40% higher distillate production to traditional stills. Rabhi et al. [35] evaluated the thermal behavior and water production efficiency of modified solar stills with pin fin absorbers and condensers, showed that the benefit of water output was significantly influenced by the presence of an external condenser. Srivastava et al. [36] studied the performance of porous fins made from blackened old cotton rags, partially submerged in basin water, which absorbed solar radiation with minimal shading, thereby increased distillate output as the water depth decreased.

Energy, exergy, environmental benefits, and economic parameters are evaluated in addition to productivity to determine economic, energy efficient and environmentally friendly solar still

[37]. The problem of unavailability of potable/hot water during night time and low efficiency of the solar thermal system at an economical cost with pollutant removal efficacy are studied by incorporating energy analysis between conventional and modified still [38]. Exergy analysis is instrumental in enhancing the actual efficiencies of thermal systems by identifying and mitigating losses and inefficiencies [39].

The above literature review highlights various techniques and design modifications aimed at enhancing the thermal efficiency and freshwater yield of solar stills. However, various fin shapes made from highly thermal conductive materials and combination of PCMs with fin yet to be tested. This type of fin-PCM integration also could reduce space for storing PCM and increase distribution area for heat transfer to basin water throughout its entire height. The incorporation of PCMs inside hollow fins could be investigated to provide immediate latent heat transfer to the entire water depth in contact with the fin surface. Therefore, this study aims to explore the effect of a hollow coil-shaped copper fin filled with PCM to achieve optimal productivity. Thus, the present study will focus on investigating the combined effect on the performance of SS for the application of coil-shaped hollow fins made of highly conductive copper with onboarded PCM. Additionally, an economic analysis is conducted to examine the cost-benefit and payback period of the solar still compared to conventional systems. A comparative analysis of critical energy, exergy, exergy-economic, and environmental parameters is also performed for those three different modifications.

2. Experimental setup and methodology

2.1 System description

An experimental test rig was developed including three differently designed Solar stills (SSs). Case -I designated as a conventional passive double slope solar still (SS), Case-II designated as a hollow copper coil fins integrated active double slope SS units, and Case-III designated as PCM filled hollow copper coil fins integrated active double slope SS units. The experimental investigations were conducted in April 2024 at the National Institute of Textile Engineering and Research (NITER), Bangladesh, situated at a geographical location of 23.7932° N latitude and 90.2713° E longitude.

The experimental setup, including the data acquisition system and controllers, was installed on the rooftop of a two-storied building to ensure the clear exposure to sunlight. The test rig was designed and fabricated to evaluate the combined effects of the proposed modifications systematically on the thermal performance and distillate yield under actual environmental conditions.

2.2 Solar Still Body Construction

Both the active modified and conventional passive solar stills (SS) possess an identical basin area of 1.1 m². The basin plates and sidewalls of the solar stills were constructed from 5.5 mm thick galvanized plain (GP) sheets, which were coated with black paint to enhance solar irradiance absorptivity and improve heat transfer to the basin water. The maximum height of the slope and the front wall of the stills are 0.45 m and 0.15 m, respectively. A 3.5 mm thick and 25° inclined glass cover serves as the condensation surface, with the inclination angle selected to match the latitude of Savar, Bangladesh. The solar stills were consistently oriented southward to maximize solar radiation exposure throughout the day. To minimize thermal losses, 20 mm thick foam insulation was applied to the base plate and sidewalls, while rubber and silicon gaskets were employed to seal the glass surfaces and edges, effectively preventing vapor leakage. In the conventional solar still (CSS), saline water was directly fed to the absorber plate at ambient temperature. In contrast, for the active solar stills, saline water was preheated using a flat plate collector (FPC), to accelerate the evaporation process prior to entering the basin plate. The saline water supply was maintained in a tank positioned 1 m above the solar stills, allowing the water to flow due to gravity. The CSS was modified with hollow coil-shaped copper fins (HCCF) and further enhanced by filling these fins with phase change material (PCM) to investigate the individual and combined effects of various design modifications. Despite both the conventional and modified solar stills sharing identical absorber plate dimensions of 1.14 m × 0.91 m, they differ significantly in absorber plate structure. The CSS features a single flat absorber plate, while the modified solar stills incorporate 60 hollow copper coil fins within the basin plate, aimed at enhancing thermal performance and distillate yield.



Fig 1. (a) Contraction of a single coil fin **(b)** Coil shaped fins placed on absorber plate

2.3 Construction of hollow copper coil fins

Construction of a single hollow fin is showed in [Fig 1](#). The hollow coil of 5 mm outer diameter, and 4 mm inner diameter was used in this study. The coil has a length (L) of 100 mm, which after being wounded, in cylindrical shape had length of 25 mm. The pitch separation between two successive HCCFs was maintained at 50 mm. The wounded cylindrical fin shaped was compared with a same diameter and length of solid cylindrical fins, the coil shaped fins provided 785.4 mm² more surface area then cylindrical shape. Therefore, the HCCFs were preferred over solid cylindrical fins as they provide excess surface area to enhance the heat transfer to the basin water. The heat transfer increased due to the close contact of the basin water with increased surface area along the whole depth of basin water. Therefore, the basin had been consistently maintained with a 25 mm water depth so that HCCFs could immerse in the water and augment the overall heat transfer co-efficient.

2.4 Arrangement for PCM

A 30 cm high single PCM reservoir had been loaded with 15 kg of paraffin wax underneath the absorber plate of modified SS to increase the reliability. For Case-III, the HCCF was connected with the PCM reservoir through opening at bottom of the coil fins for filling the inside hollow space of fins with PCM. Paraffin wax was selected due to its high latent heat of fusion, uniform melting characteristics, chemical stability, nontoxicity, low price, and safety [40]. The PCM, kept at reservoir underneath the basin, only transferred heat to lower depth of basin water which was in immediate contact with the basin. But filling the hollow fins with PCM facilitate heat transfer

to basin water throughout the whole depth of water during non-shine hours of the day and up to almost one hour after sunset.

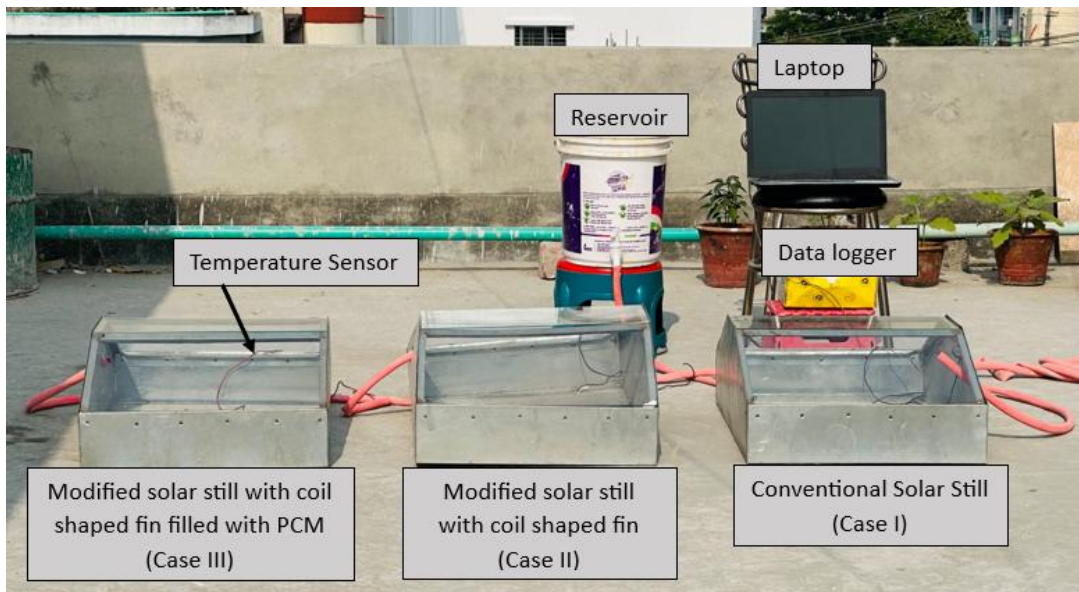
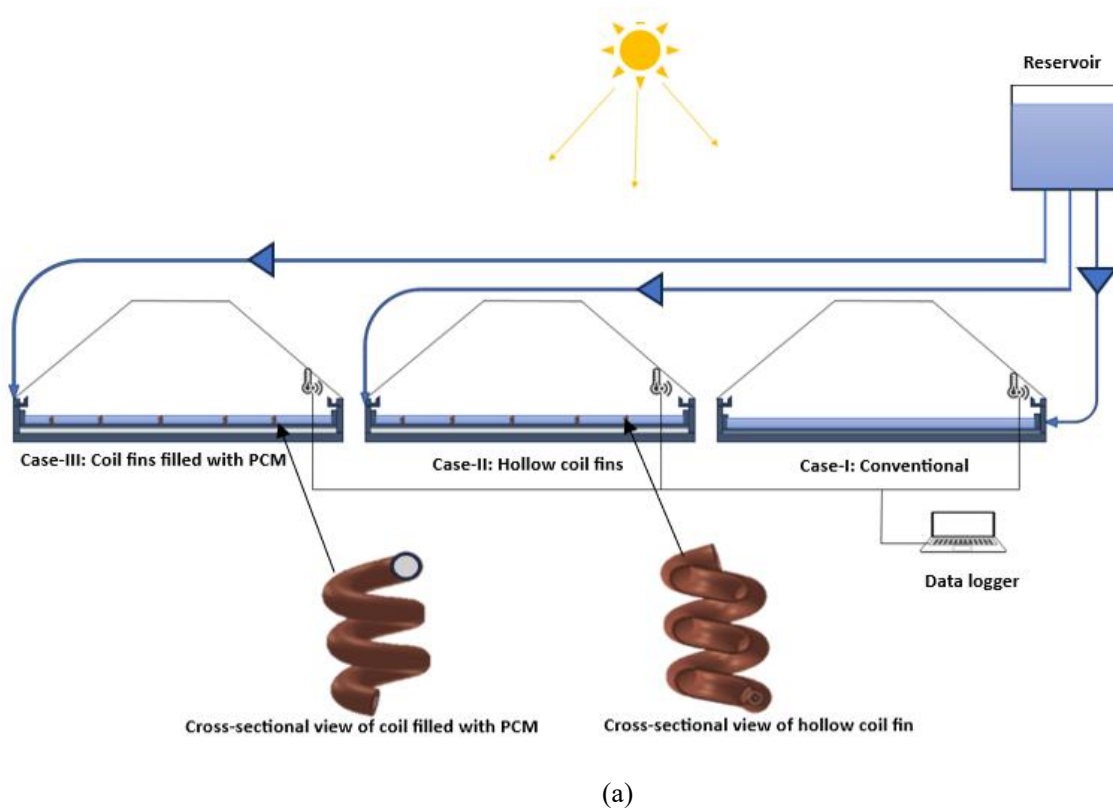


Fig 2. (a) Water flow diagram of experimental setup **(b)** Photograph of experimental setup.

2.5. Experimental methods

The experimental measurements for this study were conducted hourly from 10:00 a.m. to 7:00 p.m. The setup of the modified solar stills, highlighting all experimental configurations, is illustrated in [Fig. 2](#). Solar radiation levels were monitored using a pyranometer, capable of measuring up to 1280 W/m² within a spectral range of 300–1100 nm. Temperature readings were taken at various critical points of the solar stills, including the outer and inner glass surfaces, the basin liner, ambient air, basin water, and the PCM, using temperature sensors (Digital thermal sensor, DS18B20, Taizhou, China). These sensors were connected to a data logger (Sensors programmed on an Arduino UNO connected with laptop) for continuous recording. Wind velocity was tracked hourly with a digital vane anemometer (Vane anemometer, Fluke 925, China), while the outlet temperature of water was measured with a mercury thermometer (-10°C to 110°C range, ±1°C accuracy, Zhejiang, China). Distillate yield, produced through the condensation process, was collected in graduated beakers, and measurements were recorded each hour. The data were collected uniformly and consistently, allowing for a comprehensive performance comparison between the conventional and modified solar stills.

2.6. Uncertainty and Error Analysis

The uncertainty during the experimental process from the instruments of the solar stills (SSs) was determined using [Eq. \(1\)](#) [41].

$$u = \frac{a}{\sqrt{3}} \quad (1)$$

where "a" represents the accuracy of the instruments. In this study, DS18B20 temperature sensors were employed. Although these sensors are known for their robustness and high durability, they are still susceptible to variations caused by pressure, temperature, humidity, and vibration. The DS18B20 sensors achieved a standard uncertainty of only ±0.3°C. For measuring solar irradiation, a pyranometer (Thermopile pyranometer, Apogee Instrument, USA) was used under outdoor conditions according to ISO 9847:1992. This calibration was performed at three different locations on a sunny day with an average wind speed of 2.55 m/s. Similarly, the anemometer (Vane anemometer, Fluke 925, China) was calibrated using a pitot-tube setup prior to each measurement, also following ISO 17205:2017 standards. Detailed calibration parameters for all instruments are outlined in [Table 1](#).

Table 1 Accuracies, ranges, standard uncertainties and errors of measuring devices.

Instruments	Accuracy	Range	Standard uncertainty	% Error
Pyranometer	$\pm 1 \text{ W/m}^2$	0-2000 W/m^2	0.577 W/m^2	3.78
Temperature sensor	$\pm 0.5 \text{ }^\circ\text{C}$	-55 to 125 $^\circ\text{C}$	0.287 $^\circ\text{C}$	1.72
Vane anemometer	$\pm 0.1 \text{ m/s}$	0.25-30 m/s	0.0577 m/s	4.2
Measuring beaker	$\pm 1 \text{ ml}$	0-1000 ml	0.577 ml	1.01

2.7 Data Analyses

2.7.1 Energy Evaluation: the thermal energy efficiency of the solar still on an hourly basis was calculated using [Eq. \(2\)](#) [42].

$$\eta_{th} = \frac{m_w h_{fg}}{I_s A_b} \quad (2)$$

Where the variables are defined as follows: m_w represents the hourly freshwater yield (m^3/h), I_s stands for solar irradiation (W/m^2), A_b denotes the solar still surface area (m^2) and h_{fg} refers to the latent heat of vaporization of water (J/kg). Freshwater productivity in this study was measured hourly and was found to be dependent on the solar intensity and the modifications made for performance improvement, such as the inclusion of flat plate collectors, hollow copper coil fins (HCCF), and phase change materials (PCM). The amount of fresh water productivity depends on the solar intensity and modifications (e.g. flat plate collector, HCCF, and PCM) made for the performance improvement.

2.7.2 Exergy Analysis: Exergy analysis was performed to identify the useful work that can be extracted from the solar still when the system reaches thermodynamic equilibrium under specific conditions [43]. The exergy efficiency of the solar still as in [Eq. \(3\)](#) is determined by comparing the exergy output ($E_{x,out}$) and the exergy input ($E_{x,in}$), which are calculated using [Eq. \(4\)](#) and [\(5\)](#) [44], respectively. The exergy efficiency of the SS is given as follows:

$$\eta_{ex} = \frac{E_{x,out}}{E_{x,in}} \quad (3)$$

$$E_{x,out} = m_w h_{fg} \left[1 - \left(\frac{T_{amb}}{T_w} \right) \right] \quad (4)$$

$$E_{x,in} = I_s A_b \left[1 - \frac{4}{3} \left(\frac{T_{amb}}{T_s} \right) + \frac{1}{3} \left(\frac{T_{amb}}{T_s} \right)^4 \right] \quad (5)$$

In these equations, “ T_{amb} ” is the ambient temperature (K), and “ T_s ” is the Sun’s surface temperature (6000 K). Exergy identifies the useful attainable work from the SS when the system reaches at thermodynamic equilibrium for a given state [43].

2.7.3 Exergo-economic analysis: The exergo-economic parameter based on the exergy and energy can be calculated as follows in Eq. (6) and (7) [45],

$$R_{Ex} = \frac{Ex_{out, ann}}{TAC} \quad (6)$$

$$R_{En} = \frac{En_{out, ann}}{TAC} \quad (7)$$

where, En_{out} , and Ex_{out} are the annual energy output (kWh) and exergy output for the SS, respectively. TAC is the total annual cost (\$), FAC is the first annual cost, AMC is the annual maintenance cost and can be determined as follows in Eq. (8):

$$TAC = FAC + AMC - ASV \quad (8)$$

from the following relation in Eq. (9) [46],

$$FAC = C_c \times CRF \quad (9)$$

Here, C_c is the capital cost (\$) of the solar still and CRF is the capital recovery factor, which is obtained from Eq. (10) [47].

$$CRF(i, n) = \frac{i(1+i)^n}{(1+i)^n - 1} \quad (10)$$

Here, i and n refer to the interest rate and lifetime of the solar still respectively. AMC is taken as 10% of that of the FAC, and annual salvage value (ASV) is determined from Eq. (11):

$$ASV = S \times SFF \quad (11)$$

Here, S is the salvage value of the solar still. The value of S for the solar still is taken as 20% of the capital costs ($S = 0.2C_c$). SFF is the sinking fund factor and is determined by the following relation as in Eq. (12) [46].

$$SFF = \frac{i}{(1 + i)^n - 1} \quad (12)$$

2.7.4 Environmental impact analysis:

CO₂ emission: The CO₂ emission over the lifetime of SS is determined using [Eq. \(13\)](#).

$$X_{CO_2} = \mu_{CO_2} \times E_{in} \quad (13)$$

In above equation, μ_{CO_2} refers to the CO₂ emission factor for the electricity mix (kg/kWh). The equivalent CO₂ emission factors for the electricity mix in Bangladesh is 0.465 kg/kWh [\[48\]](#).

The overall CO₂ emission mitigation can be assessed as follows as in [Eq. \(14\)](#):

$$Y_{CO_2} = \frac{\mu_{CO_2} \times ((En_{out, ann} \times n) - E_{in})}{1000} \quad (14)$$

Carbon credit gained: Enviro-economic parameter identifies the carbon credit earned by mitigating the CO₂. The carbon credit gained is determined by the following relation as shown in [Eq. \(15\)](#) [\[42\]](#). The price of CO₂ mitigation is valued at approximately 14.5 \$/ton.

$$CCG = Y_{CO_2} \times Cost\ of\ CO_2\ traded\ per\ ton \quad (15)$$

3. Results and discussion

In this study, experimental investigations of double slope solar still with fins and PCM were performed to examine the combined effects of fins and PCM on freshwater productivity under identical weather conditions. Three different cases were considered for the analysis: Case I: conventional solar still, Case II: solar still with flat plate collector (FPC) with hollow copper coil fins (HCF), and Case III: solar still with HCF filled with PCM. The analysis includes the temperature profile and liquid yield respect to time, energy and exergy of the solar stills and economic analysis.

3.1 SS temperature profile

The temperature profiles recorded throughout 7 days for all SSs are illustrated in [Fig 3\(a\)](#), [\(b\)](#), and [\(c\)](#), respectively. During the study period, ambient temperatures ranged from 29 to 32°C, while solar intensity varied between 10 and 790 W/m² over the 9-hour measurement period on a

clear day. The temperatures of the solar still components increased progressively following the solar intensity trend as shown in [Fig. 3](#), reaching peak values at around 12:00 hours, and then gradually declined towards sunset.

For Case I, the maximum average temperatures for 7 days observed for the basin, basin water, outer glass, and inner glass surfaces were 60.6°C, 55.4°C, 42.5°C, and 49°C, respectively. The maximum average temperature difference between the inner glass surface and the basin water was 6.4°C, while the difference between the inner and outer glass surfaces was 6.5°C.

In Case II, the maximum average temperatures for the basin, basin water, outer glass, and inner glass surfaces were recorded as 60.8°C, 60.1°C, 49.5°C, and 55.5°C, respectively. While the basin temperature was almost close to that of Case I, the basin water temperature in Case II was notably higher. This increase can be attributed to the enhanced heat absorption facilitated by the extended surface area of the HCCF, which allowed the brackish water to absorb more heat from both the basin and the fins. As a result, the overall temperatures of the components in Case II remained consistently higher than those in Case I throughout the day.

In Case III, the maximum average temperatures for the basin, basin water, outer glass, inner glass, and PCM storage were 64.5°C, 63.5°C, 50.1°C, 55°C, and 58.7°C, respectively. The temperature profiles for Case III followed a similar trend to those observed in Cases I and II; however, the overall temperature values were significantly higher across all parameters.

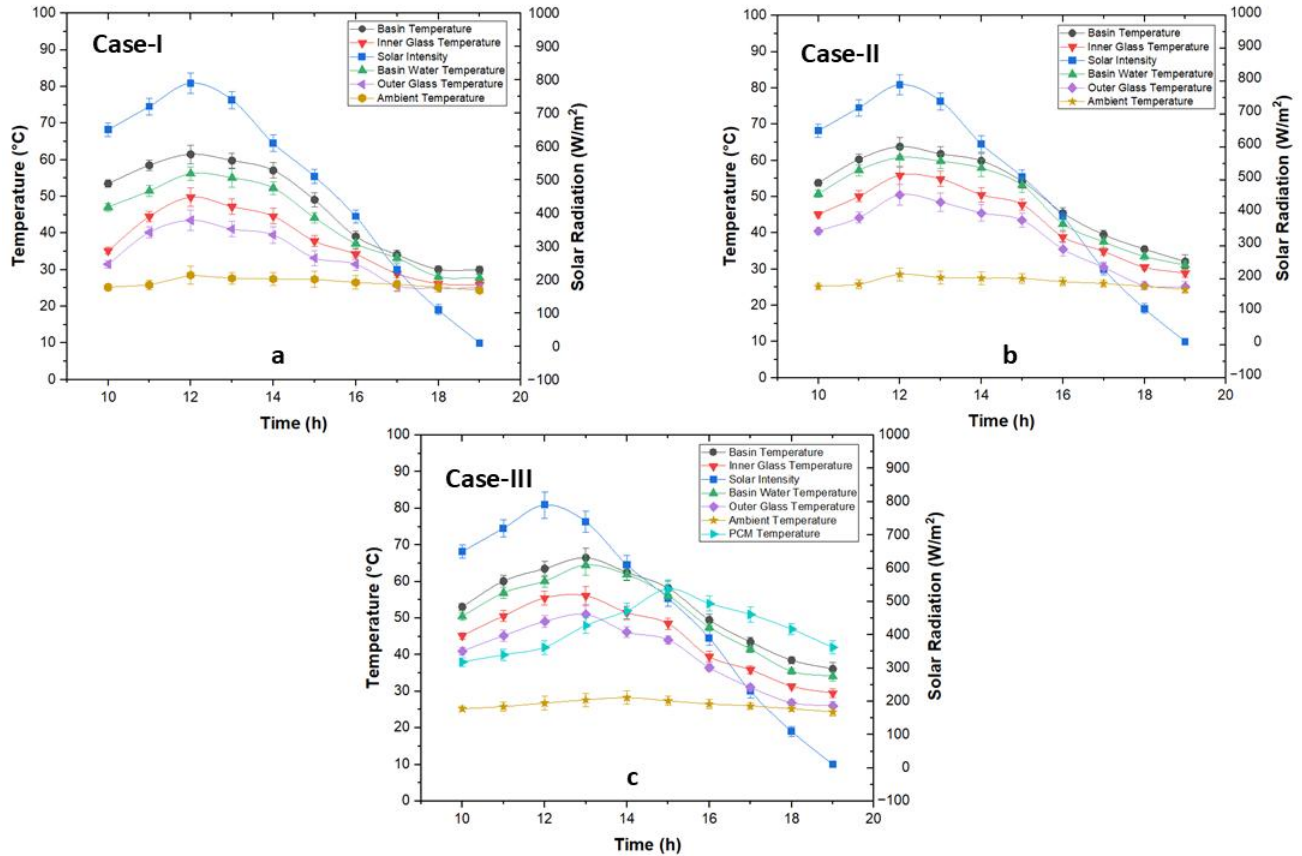


Fig. 3. Average temperature profile of 7 days for (a) Case-I, (b) Case-II and (c) Case-III.

It was observed that the peak temperature was obtained at 12:00 h for case-I and case-II, but in the case of case-III, the peak temperature was observed at 13:00 h except the temperature of the PCM. The reason is that during the initial 6 hours of the day, the basin temperature in Case III was comparatively lower due to the heat being absorbed by the PCM storage located underneath the basin and within the hollow fins. This absorbed energy was subsequently released to the basin water after 13:00 h, causing the component temperatures in Case III to surpass those of both Case I and Case II from 14:00 to 19:00 h. The PCM stored beneath the absorber plate and inside the hollow fins not only reduced heat loss from the bottom and sidewalls by absorbing excess heat but also contributed to an enhanced heat transfer coefficient. The combined effect of the additional heat from the PCM and the extended surface area of the HCCF significantly improved the thermal performance of the system. This synergy between the PCM and the HCCF facilitated a reduction in heat losses and an augmentation of the basin water temperature, thereby optimizing the solar still's efficiency through improved energy storage and heat transfer characteristics.

The error bars in the solar radiation reading curve are mainly because of the uncertainty of measuring apparatus. Error bars in the temperature curves are due to the non-uniform solar intensity and changes in wind speed during the hours of measurement throughout the 7 experimental days adding to the errors in the temperature sensors. Also, little spatial differences in temperature distribution, as well as tiny leaks or poor sealing in the solar still, could change the setup's capacity to retain heat and cause temperature fluctuations under the same circumstances, even if every experimental setup was attempted to have uniform insulation and sensors positioned in the same spot. But even with the data variations, temperature profile curves follow the same pattern in every cases. So, this little fluctuation would not affect the overall performance or efficiency.

3.2 Solar still productivity

[Fig. 4](#) illustrates the progressive distillate yield for case-I, case-II, and case-III, recorded from 10:00 h to 19:00 h. The accumulated distillate yields for cases I, II, and III were 590, 1540 and 1790 ml/day respectively. While cases I and II exhibited a flat productivity profile from 15:00 h to 19:00 h, case-III showed an upward trend during this period, resulting in the highest overall daily productivity. The distillate yield showed an increasing trend throughout the day for all cases. The water productivity for each configuration rose steadily until 13:00 h, after which cases I and II displayed a plateau. Conversely, case-III exhibited a pronounced increase in productivity from 16:00 h to 19:00 h, outperforming the other two cases.

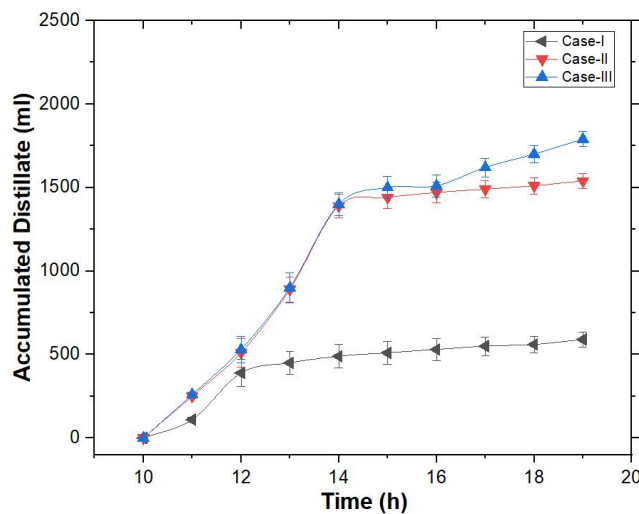


Fig. 4. Average productivity for all cases.

Case-I demonstrated the lowest productivity curve among the three configurations, attributed to the lowest basin temperature, which limited the evaporation rate. Case-II achieved higher productivity than case-I due to an improved evaporation rate resulting from increased basin temperatures. However, case-III achieved the highest productivity among all configurations. This enhanced performance of case-III can be attributed to the higher basin temperatures observed during both peak solar radiation hours and non-sunshine hours, facilitated by the extended surface area provided by HCCF and Phase Change Material (PCM). The reason was the facilitation of heat transfer by the PCM inside the hollow fins which were in the immediate contact throughout the whole depth of basin water. Thus, case-III proved to be the most effective configuration in enhancing solar still productivity.

Since these are averages of the values of 7 experimental days, error bars in the graph resulted from fluctuations in evaporation and condensation rates due to inconsistent solar irradiance and shadow patterns affecting the thermal gradient. Variability in moisture content within the basin, influenced by ambient humidity and wind speed also had variation during certain measuring hours throughout different experimental days. Additionally, minor inconsistencies in the phase change dynamics of the PCM and its interaction with the basin water had contributed to deviations in the distillate yield.

3.3 Energy analysis

[Fig 5\(a\)](#) shows the efficiency variations of the solar stills throughout the day for each case. The peak average energy efficiencies recorded for cases I, II, and III were 22.9%, 27.3%, and 37.5%, respectively. In [Fig 5\(b\)](#), the daily average overall efficiency of the solar still for case-III surpassed that of cases I and II by 122.22 % and 68 %, respectively.

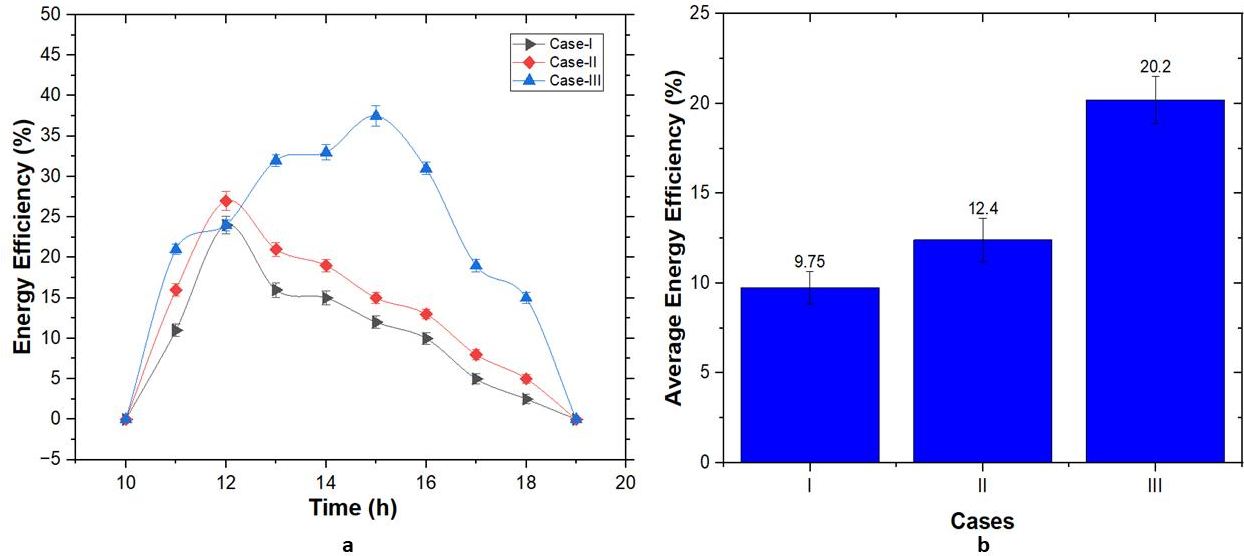


Fig. 5. (a) Hourly and (b) daily average energy efficiency for all cases

The energy efficiency of the solar stills for all cases was determined using [Eq. \(2\)](#). Given the identical still area and incident solar radiation, efficiency is primarily influenced by the distillate productivity and the temperature gradient between the inner glass surface and the basin water. Case-I exhibited significantly lower efficiency compared to cases II and III, mainly due to higher heat losses and lower basin water temperatures, which hindered evaporation. Maximum efficiency was reached at 13:00 h for cases I and II, while for case-III, it was delayed until 15:00 h. This delay in case-III can be attributed to the time required for the PCM to absorb and release energy effectively at its peak temperature as seen from [Fig 3\(c\)](#). During peak solar intensity at 13:00 h, case-III's efficiency lagged due to PCM's thermal response time.

Case-III achieved an average maximum efficiency of 20.2 % highest among all modifications due to the enhanced energy retention and dissipation provided by the PCM, which facilitated greater evaporation rates. This superior performance in case-III is directly linked to improved evaporation rates, resulting in significantly higher productivity, making it the most efficient configuration among the three. Case-III's superior energy efficiency can also be attributed to the PCM's ability to minimize temperature fluctuations in the basin water during day and at night, PCM's thermal storage capacity allows it to store excess heat during peak solar hours and release it during lower irradiance periods, extending the effective operational time of the system. Additionally, the hollow coil fins filled with PCM enhanced heat transfer efficiency by maintaining a higher localized temperature gradient at immediate contact surface of water. This

synergistic effect between the PCM and hollow fins reduced overall heat losses, optimizing energy utilization.

Errors in the curve can be attributed to the reason that solar irradiation variation occurred rapidly due to intermittent cloud cover, leading to short-term fluctuations in recorded energy efficiency, even if the system performance remains steady.

3.4 Exergy analysis

From [Fig 6 \(a\)](#) it is seen that Case I exhibited the lowest ratio of amount of useful energy output by the total amount of energy input, with a maximum average value of 1.65 %. Case II showed an improvement, with a maximum average value of 3.4 %. Case III achieved the highest exergy efficiency, with a maximum average value of 4.25 %. The data illustrated in [Fig 6 \(b\)](#) confirm that Case III exhibited approximately 333.33 % and 108 % higher daily average exergy efficiency compared to Case I and Case II respectively.

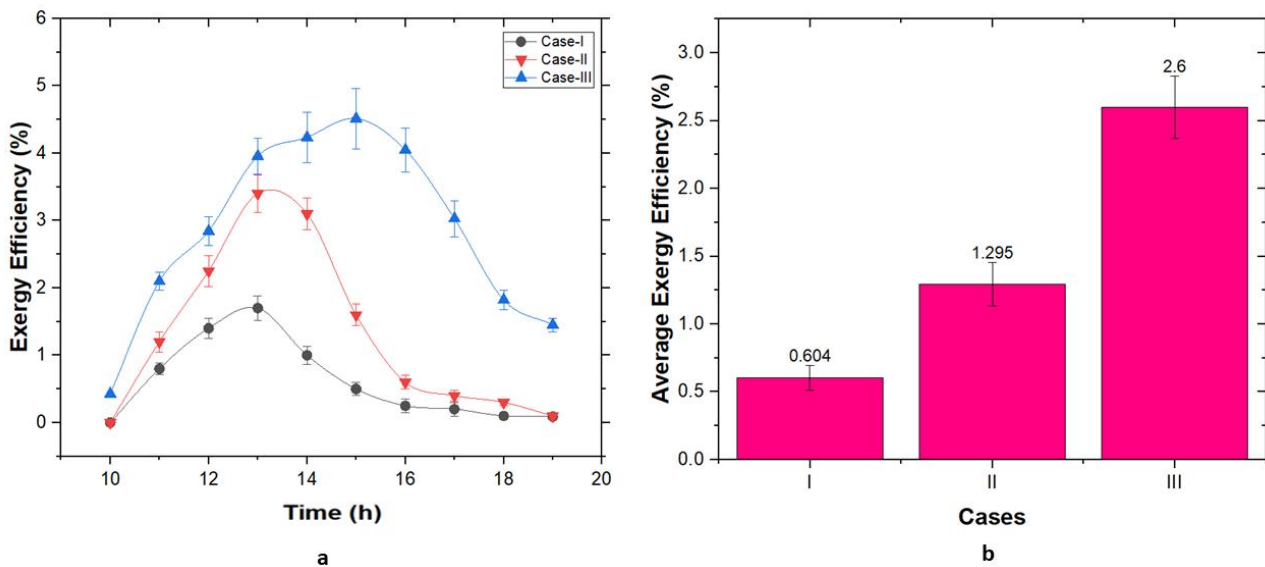


Fig. 6. (a) Hourly and (b) daily average exergy efficiency for all cases.

The exergy efficiency of the solar stills was evaluated across three different cases using [Eq. \(3\)](#), with the ambient temperature, basin water temperature, and productivity being the primary variables of interest. The maximum average temperature differences between the ambient temperature and basin water temperatures were found to be 23.4°C, 28.1°C, and 31.5°C for Case I, Case II, and Case III, respectively as seen from the temperature profiles in [Fig 3](#). This temperature difference is a critical factor influencing the exergy efficiency of the solar stills. For

case-I, lowest average basin water temperature among the cases was observed, resulting in minimal temperature differences and therefore, reduced evaporation rates and exergy output. For case-II, the use of coil-shaped fins provided an extended surface area for heat transfer, which led to a higher basin water temperature compared to Case I. This increase in temperature difference between the basin water and ambient environment improved the evaporation rate and, consequently, the exergy efficiency. Case-III incorporated hollow coil-shaped fins filled with Phase Change Material (PCM), which not only enhanced heat transfer during sunlight hours but also provided additional heat during non-shine hours. As a result, the basin water temperature in Case III was the highest among all cases, leading to the maximum evaporation rate and productivity. The consistent ambient temperature across all cases ensured that the variations in exergy efficiency were primarily due to the differences in basin water temperatures and productivity enhancements. Case-III's superior exergy efficiency could be attributed to the PCM's ability to sustain higher basin water temperatures for prolonged periods, maximizing the availability of useful energy (exergy) for evaporation.

Error bars in the evaluation of exergy efficiency for the solar stills could result from several factors, including measurement uncertainties, environmental fluctuations, and material variations. Inaccuracies in temperature sensor readings and productivity measurements can introduce discrepancies, while microclimatic variations such as slight changes in solar radiation, wind speed, or humidity could affect thermal performance. Variations in the thermal properties of materials like the coil-shaped fins and PCM could influence heat transfer rates and energy conversion efficiency, contributing to differences in temperature profiles and productivity. These combined factors result in deviations in exergy efficiency, reflected by the error bars in the data.

3.5 Economic analysis

The cost of water (COW) is a crucial factor in evaluating the economic viability of solar stills. According to our study, Case III, which demonstrates the highest energy efficiency and productivity, also presents a competitive economic profile despite higher initial costs. [Table 2](#) shows that Case III incurs a higher cost for PCM and HCCF, but its increased freshwater production offsets this expense. Consequently, Case III exhibits a shorter payback period of 288 days compared to 424 days for Case I and 305 days for Case II, as shown in [Table 3](#).

Table 2 Cost analysis of different SS cases:

Parameters	Case-I	Case-II	Case-III
n (yr)	20	20	20
i (interest rate %)	0.1	0.1	0.1
CRF	0.1175	0.1175	0.1175
Cc (Capital cost \$)	55	110	121
S	11.1	22.2	24.1
FAC	6.91	12.31	14.1
SFF	0.0175	0.0175	0.0175
ASV	0.195	0.410	0.470
AMC	0.6985	1.654	1.985
TAC	7.111	13.955	14.528
M_{wp} (L/yr)	352.21	645.52	710.53
COW (\$/L)	.0210	.0205	0.0187

Table 3 Calculation of payback time of SS cases

Parameters	Case-I	Case-II	Case-III
Cc (capital cost \$)	55	110	121
Average yield per day (L/m²)	0.59	1.540	1.790
Gain (Avg. Yield x market price) (\$/m²/day)	0.13	0.35	0.42
Payback time (Cc/Gain) (days)	424	305	288

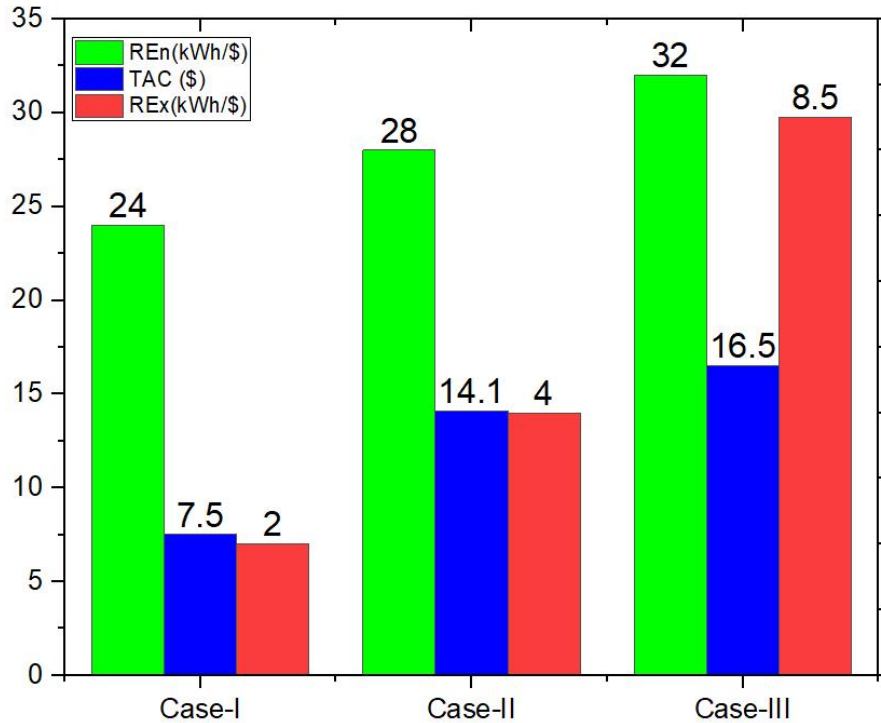


Fig. 7. Economic parameters and total annual cost for all three cases.

The economic performance of the solar stills was assessed using both exergo-economic parameters and the total annual cost. The results indicate that Case III, while having a higher initial investment due to the cost of PCM and HCCF, offers substantial economic benefits through enhanced productivity. [Fig. 7](#) illustrates that although the total annual cost for Case III is higher than for Cases I and II, this is balanced by its superior performance in terms of yearly energy output and exergy output.

3.6 Environmental impact

The environmental feasibility of the solar stills was assessed using three key parameters: carbon dioxide (CO₂) emissions, CO₂ mitigation, and carbon credits. [Fig. 8](#) provides a comprehensive overview of these aspects for the different solar stills. For case-I, conventional solar still has the simplest design and results in the lowest embodied CO₂ emissions of 300 kg. For case II, this design is slightly more complex with HCCF and emits 900 kg CO₂. While Case III, with its advanced design including HCCF and PCM filled in HCCF, has highest 1200 kg CO₂ emission among all.

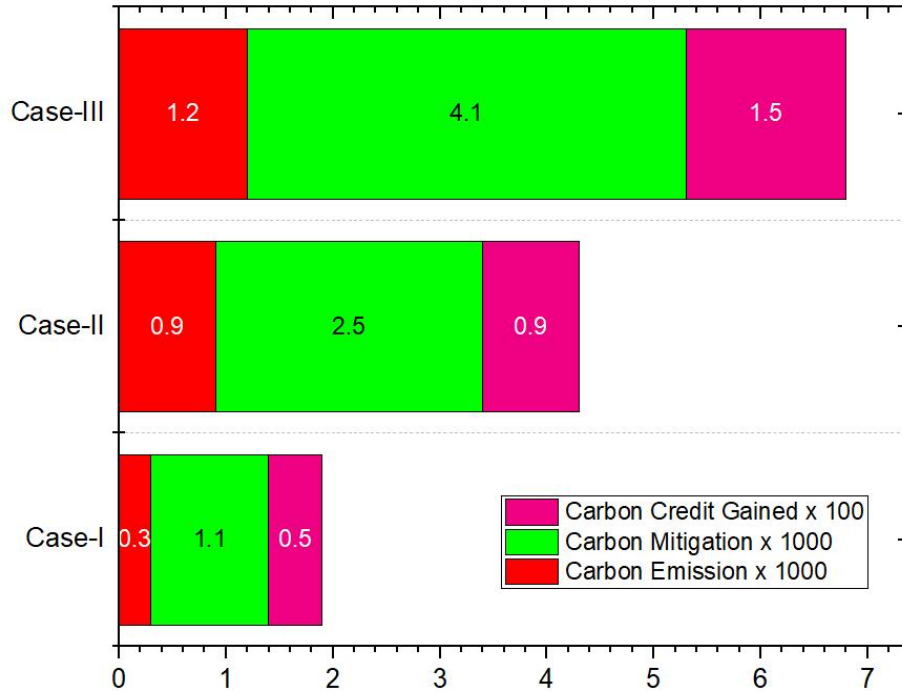


Fig. 8. Carbon emission, mitigation and carbon credit gained for all three cases.

All solar stills under study are operationally CO₂ neutral, meaning they do not produce CO₂ during their use. However, the manufacturing process of the materials used—such as steel frames, glass covers, basin plates, PCM, and insulation does involve CO₂ emissions due to the electricity used, which often comes from fossil fuels. Despite the higher embodied CO₂ emissions due to more complex design, Case III provides the highest CO₂ mitigation during its operational period. Case III mitigates a maximum of 4.1 tons of CO₂, which is 1.6 tons more than Case II and 3 tons more than Case I. This is because the additional features in Case III enhance its efficiency, leading to greater overall energy output and more effective CO₂ reduction. Case III, with its higher CO₂ mitigation and energy output, can earn \$150 in carbon credits. This is \$60 more than Case II and \$100 more than Case I. This demonstrates that the environmental benefits of Case III outweigh its initial CO₂ footprint, making it a strong choice from an environmental perspective.

4. Conclusions

This study experimentally tested the performance of a double slope solar stills (SS) by integrating a PCM filled hollow copper coiled fin to improve freshwater productivity and overall

efficiency. The research also included a comprehensive study of experimental setup by analyzing its energy, exergy, economic, and environmental impact. Among the tested configurations, Case III (PCM filled hollow circular fins integrated solar still) demonstrated significantly improved heat retention and transfer, resulting in higher basin and basin water temperatures, particularly during peak and non-peak solar hours. This modification achieved the highest daily distillate production of 1790 ml, the maximum average energy efficiency of 37.5%, and the peak average exergy efficiency of 4.25%. Despite its higher initial cost, Case III demonstrated economic feasibility with a payback period of 288 days, which was the shortest among the cases, and a lower long-term cost of water production. Environmentally, Case III showcased the greatest CO₂ mitigation potential, offsetting up to 4.1 tons of emissions and earning \$150 in carbon credits, thereby compensating for its embodied CO₂ emissions during manufacturing. The findings underscore the potential of advanced configurations like Case III in using an efficient way of PCM along with fins. This study highlights the importance of integrating innovative materials and designs for efficient freshwater production, especially in coastal regions where access to clean water is vital for sustainable development.

Acknowledgement

The authors would like to express sincere gratitude to the authority of National Institute of Textile and Research Engineering for the technical supports during the experimentation process.

Nomenclature

A_b	Solar still area (m ²)
a	Accuracy of instruments
C_c	Capital cost (\$)
E_{in}	Embodied energy (kWh)
$E_{x, in}$	Exergy input (kWh)
$E_{x, out}$	Exergy output (kWh)
E_{Xwaste}	Waste energy (kWh)

$EX_{out, ann}$	Annual output exergy (kWh)
$En_{out, ann}$	Annual output energy (kWh)
h_{fg}	Latent heat of evaporation of water (J/kg)
I_s	Solar irradiation (W/m^2)
i	Interest rate (%)
m_w	Freshwater productivity (m^3/h)
n	Life time of solar still (yr)
R_{En}	Exergo-economic parameter based on energy (kWh/\$)
R_{Ex}	Exergo-economic parameter based on exergy (kWh/\$)
S	Salvage value (\$)
T_{amb}	Ambient temperature (K)
T_s	Sun temperature (K)
T_w	Basin water temperature (K)
X_{CO_2}	CO ₂ emission over the lifetime of solar still

Abbreviations

AMC	Annual maintenance cost (\$)
ASV	Annual salvage value (\$)
CRF	Capital recovery factor
COW	Cost of water (\$/L)
CCG	Carbon credit gained (\$)
EEF	Environmental effect factor
FAC	First annual cost
IP	Improvement potential (kWh/yr)
SI	Sustainability index

SFF Sinking fund factor

TAC Total annual cost

References

- [1] W.L. Seri, Solar Energy Water Desalination in the United States and Saudi Arabia, (1981).
- [2] Mohan, S. Yadav, H. Panchal, S. Brahmabhatt, A review on solar still: a simple desalination technology to obtain potable water, *Int. J. Ambient Energy*, vol. 40, pp. 335–342, 2019.
- [3] M.M. Elsayed, Comparison of transient performance predictions of a solar-operated diffusion-type still with a roof-type still, *J. Solar Energy Eng.*, vol. 105, pp. 23–28, 1983.
- [4] S. Kumar and G.N. Tiwari, Optimization of collector and basin areas for a higher yield for active solar stills, *Int. J. Desalination*, vol. 116, pp. 42–54, 1998.
- [5] P. Vishwanath Kumar, Anil Kumar, Om Prakash, Ajay Kumar Kaviti, Solar stills system design: A review, *Renew. Sustain Energy Rev.*, vol. 51, pp. 153–181, 2015.
- [6] H.N. Panchal, Experimental Analysis of different absorber plates on the performance of Double slope solar Still, *Int. J. Eng. Sci. Technol.*, vol. 2, pp. 6626–6629, 2010.
- [7] S.W. Sharshir, N. Yang, G. Peng, A.E. Kabeel, Factors affecting solar stills productivity and improvement techniques: a detailed review, *Appl. Therm. Eng.*, vol. 100, pp. 267–284, 2016.
- [8] Karthikeyan Selvaraj, Alagumurthi Natarajan, Factors influencing the performance and productivity of solar stills-A review, *Desalination*, vol. 435, pp. 181–187, 2018.
- [9] K. Elmaadawy et al., Performance improvement of double slope solar still via combinations of low-cost materials integrated with glass cooling, *Desalination*, vol. 500, p. 114856, 2021.
- [10] K.H. Nayi and K.V. Modi, Pyramid solar still: a comprehensive review, *Renew. Sustain. Energy Rev.*, vol. 81, pp. 136–148, 2018.
- [11] Kabeel, Z. Omara, M. Younes, Techniques used to improve the performance of the stepped solar still—a review, *Renew. Sustain. Energy Rev.*, vol. 46, pp. 178–188, 2015.
- [12] F. Essa et al., Experimental investigation of convex tubular solar still performance using wick and nanocomposites, *Case Stud. Therm. Eng.*, vol. 27, p. 101368, 2021.
- [13] S.W. Sharshir et al., Improving the performance of tubular solar still integrated with drilled carbonized wood and carbon black thin film evaporation, *Sol. Energy*, vol. 233, pp. 504–514, 2022.

- [14]K.V. Modi, K.H. Nayi, S.S. Sharma, Influence of water mass on the performance of spherical basin solar still integrated with parabolic reflector, *Groundwater for Sustainable Development*, vol. 10, p. 100299, 2020.
- [15]Z. M. Omara, A. E. Kabeel, and M. M. Younes, "Enhancing the stepped solar still performance using internal and external reflectors," *Energy Conversion and Management*, vol. 78, pp. 876-881, Feb. 2014.
- [16]Kabeel and M. Abdelgaied, Enhancement of pyramid-shaped solar stills performance using a high thermal conductivity absorber plate and cooling the glass cover, *Renew. Energy*, vol. 146, pp. 769–776, 2020.
- [17]Sarbu and C. Sebarchievici, A comprehensive review of thermal energy storage, *Sustainability*, vol. 10, no. 1, p. 191, 2018.
- [18]T. Kousksou, P. Bruel, A. Jamil, T. El Rhafiki, and Y. Zeraouli, Energy storage: applications and challenges, *Sol. Energy Mater. Sol. Cells*, vol. 120, pp. 59–80, 2014.
- [19]P. Prakash and V. Velmurugan, Parameters influencing the productivity of solar stills a review, *Renew. Sustain. Energy Rev.*, vol. 49, pp. 585–609, 2015.
- [20]K.Y. Leong, M.R.A. Rahman, and B.A. Gurunathan, Nano-enhanced phase change materials: a review of thermo-physical properties, applications and challenges, *J. Energy Storage*, vol. 21, pp. 18–31, 2019.
- [21]H. Nazir et al., Recent developments in phase change materials for energy storage applications: a review, *Int. J. Heat Mass Transf.*, vol. 129, pp. 491–523, 2019.
- [22]W. Wang et al., Fe₃O₄-functionalized graphene nanosheet embedded phase change material composites: efficient magnetic- and sunlight-driven energy conversion and storage, *J. Mater. Chem. A*, vol. 5, pp. 958–968, 2017.
- [23]Y. Zhang et al., Ultrafast and efficient photothermal conversion for sunlight-driven thermal-electric system, *Chem. Eng. J.*, vol. 344, pp. 402–409, 2018.
- [24]L. Xie et al., Review on application of phase change material in water tanks, *Adv. Mech. Eng.*, vol. 9, no. 7, pp. 1–13, 2017.
- [25]A. A. Masood, "A Study on the Challenges and Prospects of PCM Based Main Memory Architectures," *Middle East Journal of Scientific Research*, vol. 18, no. 6, pp. 788-795, Dec. 2013.

- [26] M. Jahanpanah et al., Experimental investigation of the effects of low-temperature phase change material on single-slope solar still, *Desalination*, vol. 499, p. 114799, 2021.
- [27] Kabeel et al., Experimental study on tubular solar still using Graphene Oxide Nano particles in Phase Change Material (NPCM's) for fresh water production, *J. Energy Storage*, vol. 28, p. 101204, 2020.
- [28] H.M. Maghrabie et al., Phase change materials based on nanoparticles for enhancing the performance of solar photovoltaic panels: a review, *J. Energy Storage*, vol. 48, p. 103937, 2022.
- [29] M.R. Safaei, H.R. Goshayeshi, and I. Chaer, Solar still efficiency enhancement by using graphene oxide/paraffin nano-PCM, *Energies*, vol. 12, no. 10, p. 2002, 2019.
- [30] A.A. El-Sebaili and M. El-Naggar, Year-round performance and cost analysis of a finned single basin solar still, *Applied Thermal Engineering*, vol. 110, pp. 787–794, 2017.
- [31] V. Velmurugan, C. Deenadayalan, H. Vinod, et al., Desalination of effluent using fin type solar still, *Energy*, vol. 33, no. 11, pp. 1719–1727, 2008.
- [32] T. Rajaseenivasan, P.N. Raja, and K. Srithar, An experimental investigation on a solar still with an integrated flat plate collector, *Desalination*, vol. 347, pp. 131–137, 2014.
- [33] A.A. El-Sebaili and S.M. Shalaby, Parametric study and heat transfer mechanisms of single basin v-corrugated solar still, *Desalination and Water Treatment*, vol. 55, no. 2, pp. 285–296, 2015.
- [34] Z.M. Omara, M.H. Hamed, and A.E. Kabeel, Performance of finned and corrugated absorbers solar stills under Egyptian conditions, *Desalination*, vol. 277, no. 1–3, pp. 281–287, 2011.
- [35] K. Rabhi, R. Nciri, F. Nasri, C. Ali, and H. Ben Bacha, Experimental performance analysis of a modified single-basin single-slope solar still with pin fins absorber and condenser, *Desalination*, vol. 416, pp. 86–93, 2017.
- [36] P.K. Srivastava and S.K. Agrawal, Winter and summer performance of single sloped basin type solar still integrated with extended porous fins, *Desalination*, vol. 319, pp. 73–78, 2013.
- [37] H. Sharon, Energy, exergy, environmental benefits and economic aspects of novel hybrid solar still for sustainable water distillation, 2021.
- [38] A.K. Pathak, V.V. Tyagi, K. Chopra, M. Sharma, S. Anand, R. Kothari, and A.K. Pandey, Energy, exergy, and economic analysis of solar still integrated with phase change material

- assimilated evacuated tube collector for wastewater treatment, *Energy*, vol. 193, pp. 1300–1319, 2025.
- [39] Kabeel, G.B. Abdelaziz, and E.M. El-Said, Experimental investigation of a solar still with composite material heat storage: energy, exergy and economic analysis, *Journal of Cleaner Production*, vol. 231, pp. 21–34, 2019.
- [40] M.S. Yousef and H. Hassan, An experimental work on the performance of single slope solar still incorporated with latent heat storage system in hot climate conditions, *Journal of Cleaner Production*, vol. 209, pp. 1396–1410, 2019.
- [41] J. Taylor, *Introduction to Error Analysis: The Study of Uncertainties in Physical Measurements*, 2nd ed. Sausalito, CA, USA: University Science Books, 1997.
- [42] M.S. Yousef, H. Hassan, and H. Sekiguchi, Energy, exergy, economic and enviro-economic (4E) analyses of solar distillation system using different absorbing materials, *Applied Thermal Engineering*, vol. 150, pp. 30–41, 2019.
- [43] M.S. Yousef and H. Hassan, Energy payback time, exergo-economic and enviro-economic analyses of using thermal energy storage system with a solar desalination system: an experimental study, *Journal of Cleaner Production*, vol. 270, p. 122082, 2020.
- [44] S. Sharshir et al., Thermal performance and exergy analysis of solar stills—A review, *Renewable and Sustainable Energy Reviews*, vol. 73, pp. 521–544, 2017.
- [45] S. Shoeibi et al., Energy matrices, exergoeconomic and enviro-economic analysis of air-cooled and water-cooled solar still: experimental investigation and numerical simulation, *Renewable Energy*, vol. 171, pp. 227–244, 2021.
- [46] S. Nazari, H. Safarzadeh, and M. Bahiraei, Performance improvement of a single slope solar still by employing thermoelectric cooling channel and copper oxide nanofluid: an experimental study, *Journal of Cleaner Production*, vol. 208, pp. 1041–1052, 2019.
- [47] B.K. Das et al., Techno-economic and environmental assessment of a hybrid renewable energy system using multi-objective genetic algorithm: a case study for remote Island in Bangladesh, *Energy Conversion and Management*, vol. 230, p. 113823, 2021.
- [48] S.K. Nandi and H.R. Ghosh, Prospect of wind–PV–battery hybrid power system as an alternative to grid extension in Bangladesh, *Energy*, vol. 35, no. 7, pp. 3040–3047, 2010.